Ultrafast carrier dynamics in Br^+-bombarded InP studied by time-resolved terahertz spectroscopy

H. Němec, L. Fekete, F. Kadlec, and P. Kužel
Institute of Physics, Academy of Sciences of the Czech Republic, Na Slovance 2, 182 21 Prague 8, Czech Republic

M. Martin and J. Mangeney
Institut d'Electronique Fondamentale, Université Paris XI, UMR CNRS 8622, 91405 Orsay Cedex, France

J. C. Delagnes and P. Mounaix
Centre de Physique Moléculaire Optique et Hertzienne, Université Bordeaux I, UMR CNRS 5798, 351 Cours de la Libération, 33405 Talence Cedex, France

(Received 15 September 2008; revised manuscript received 27 November 2008; published 29 December 2008)

Ultrafast dynamics of charge carriers in Br^+-bombarded InP were studied using time-resolved terahertz spectroscopy. Carrier lifetimes and mobilities in various samples prepared with irradiation doses spanning from 10^9 up to 10^{12} cm^{-2} were determined. The lifetime of photoexcited carriers appears to be determined primarily by the density of defects resulting from host-atom displacements while it is not significantly influenced by the Br-atom implantation. In the most irradiated sample, a carrier lifetime as short as 300 fs was found. All samples exhibit a high mobility ($3000-900$ cm^2 V^{-1} s^{-1}); the lower values correspond to a smaller irradiation dose. In selected samples, the density of traps along with electron and hole lifetimes was determined.

DOI: 10.1103/PhysRevB.78.235206 PACS number(s): 78.47.J−, 71.55.Eq

I. INTRODUCTION

The ongoing progress in the development of ultrafast optoelectronic devices requires materials satisfying the simultaneous demands for ultrashort carrier lifetime, high mobility, and high dark resistivity.[1] Low-temperature-grown gallium arsenide (GaAs) is an important material displaying, to a large extent, these properties.[2] Several studies have been performed to achieve similar characteristics in InP since this material is widely used in high-speed electronic and optoelectronic components. However, in contrast to GaAs, the growth of InP at low temperature produces a highly conductive material due to ionized phosphorus antisite defects[3]

Much better optoelectronic properties are found in ion-bombarded InP.[4–6] In particular, interesting optoelectronic properties are produced by bombarding InP by ions with a high initial energy[4,5] which generates only host-atom displacements near the wafer surface while ions used for the bombardment are implanted a few microns below the wafer surface.[7] Depending on the ion mass of the irradiating particle, the produced defects are different. Light ion (e.g., proton) irradiation creates only isolated point defects whereas heavy-ion irradiation creates defect clusters in addition to point defects. The electrical and optical properties are governed by the specific defect nature.[8]

The dynamics of charge carriers in proton-irradiated InP were investigated previously using time-resolved terahertz spectroscopy.[9] This technique is a powerful contact-free method suitable for the characterization of optoelectronic properties of semiconductors,[10,11] yielding transient terahertz conductivity spectra of optically excited samples. Thus it is possible to monitor the evolution of both concentration and mobility of charge carriers with a subpicosecond temporal resolution.[12,13]

In this paper, we present a detailed time-resolved terahertz spectroscopy study of the effect of heavy-ion (Br^+) irradiation of InP wafers on the behavior of photocarriers. In III-V semiconductors, heavy-ion irradiation creates essentially clusters of point defects.[8] Transient far-infrared conductivity of the ion irradiated samples was measured and analyzed in order to determine the carrier lifetimes and mobilities. We also propose a dynamical model accounting for both trap filling and carrier diffusion, which made it possible to evaluate density of traps along with electron and hole lifetimes for selected samples.

II. SAMPLES

We investigated two sets of ⟨100⟩-oriented InP wafers irradiated by 11 MeV Br^+ ions in order to study the influence of host-atom defects and of Br-atom implantation. The samples in the first set were obtained from bare InP wafers irradiated at doses of 10^9, 10^{10}, 10^{11}, and 10^{12} cm^{-2} (these will be referred to as B9–B12 samples). The second set of samples consisted of InP wafers initially covered with an epitaxially grown 3 μm thick $In_{0.53}Ga_{0.47}As$ film. After Br^+ irradiation at doses of 10^9, 10^{10}, and 10^{11} cm^{-2}, the $In_{0.53}Ga_{0.47}As$ layer was removed by a wet selective chemical etching in $H_3PO_4/H_2O_2/H_2O$, leaving the bare irradiated InP substrate (these samples are labeled as E9–E11). As explained below, these two different preparation methods allow us to investigate irradiated regions with different ratios of implanted-ion/host-atom defect concentrations ratio in order to elucidate their respective contributions.

The "stopping range of ions in the matter" (SRIM) software[14] was used to calculate the depth profiles of Br-atom implantation density and the profile of density of host-atom displacement defects (Fig. 1). Since only a thin surface layer ($1/\alpha=300$ nm) of InP was excited by optical pump pulses in our experiments, we probe a region free of Br implantation in the B samples, while the depth containing nearly the maximum density of Br atoms was probed in the E samples. Note that the density of host-atom displacements in

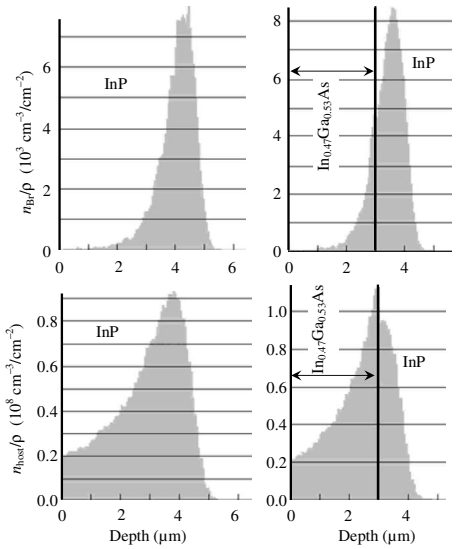

FIG. 1. Depth profiles of calculated Br-atom implantation densities n_{Br} (top panels) and densities of host-atom displacement defects n_{host} (bottom panels). Left panels show the profiles in bulk InP (B samples), while the right panels display the densities in InP overlaid with the 3 μm thick $In_{0.47}Ga_{0.53}As$ film (E samples). The densities are normalized by the irradiation dose ρ. The step at the $In_{0.47}Ga_{0.53}As/InP$ interface originates from different projected ranges of the Br^+ ions, which are related to mass densities of InP (4.8 g cm^{-3}) and $In_{0.47}Ga_{0.53}As$ (5.5 g cm^{-3}). The photoexcited surface is located at 0 and 3 μm for B and E samples, respectively.

the E9–E11 samples was higher by a factor of 4.5 as compared to the B9–B11 samples prepared using the same irradiation dose.

III. EXPERIMENTAL METHODS

The transient terahertz conductivity was measured in a usual setup for optical pump-terahertz probe experiments[11] driven by a Ti:sapphire laser amplifier (810 nm mean wavelength, 55 fs pulse width, 1 kHz repetition rate, and energy of 1 mJ per pulse). In brief, terahertz pulses were generated by optical rectification in a 1 mm thick (110) ZnTe crystal and detected by means of electro-optic sampling in another (110) ZnTe crystal, thus covering a spectrum from ~0.2 to ~2.5 THz. Excitation of the InP wafers was accomplished by the 810 nm pulses attenuated to achieve excitation densities of about 10^{17} cm^{-3}.

The aim of the optical pump-terahertz probe experiments was to determine the time-dependent spectra of the transient photoconductivity $\Delta\sigma(f,\tau_p)$ (f is the probing terahertz frequency and τ_p is the pump-probe delay) bearing information about carrier lifetimes and mobilities. For this purpose, it is necessary to measure the photoinduced modification $\Delta E(f,\tau_p)$ of the terahertz spectrum transmitted through the sample (so-called transient spectrum), and the spectrum $E(f)$ transmitted through the unexcited sample. As long as the investigated photoinitiated dynamics is slow compared to the terahertz pulse length (~1.5 ps; this is satisfied for the E9, E10, and B9–B11 samples), a quasistatic approximation can be applied. This approximation assumes that the state of the photoexcited sample does not change within the probing event. In the small-signal limit ($\Delta E \ll E$), the surface transient conductivity actually probed then reads[15,16]

$$\Delta S(f,\tau_p) = -2\varepsilon_0 c(1+N)\frac{\Delta E(f,\tau_p)}{E(f)}, \tag{1}$$

where ε_0 is the permittivity of vacuum, c is the speed of light in vacuum, and N is the far-infrared refractive index of InP. The value of the bulk transient conductivity $\Delta\sigma(f,\tau_p)$ at the sample surface is then simply $\Delta S(f,\tau_p)$ scaled by the absorption coefficient α at the excitation wavelength.

In parallel, we also measured the photoinduced change at the maxima of the terahertz wave forms as a function of the pump-probe delay (so-called pump-probe scan), which represent spectrally unresolved (averaged) information about the photoinitiated dynamics. The investigation of dynamics on timescales comparable with or shorter than the terahertz pulse length (the E11 and B12 samples) requires applying more advanced methods in the data analysis. In particular, it is essential to take into account the frequency mixing of the terahertz radiation with the spectral content of the evolution of the far-infrared response function and to deconvolute correctly the detector response.[17,18] Here we follow an approach based on the Fourier transformation into two-dimensional frequency domain, which makes it possible to determine the transient photoconductivity $\Delta\sigma(f,f_p)$ analytically, without relying on extensive modeling.[15,18] The frequency f_p is the Fourier-conjugated variable to the pump-probe delay τ_p and it describes the dynamics of the excited system. The experimental procedure and data analysis are described in detail in Ref. 13. Note that the region accessible in the (f,f_p) spectral plane is limited especially by the bandwidth of the emitter and detector.[18]

IV. EXPERIMENTAL RESULTS

As an example transient conductivity spectra of the E9 and E10 samples are shown in Fig. 2(a) for a few representative pump-probe delays. The spectra clearly exhibit a Drude response of free charge carriers,[19]

$$\Delta\sigma(f,\tau_p) = \frac{n(\tau_p)e_0^2}{m_{\text{eff}}}\frac{\tau_s}{1-2\pi i f\tau_s}, \tag{2}$$

where $n(\tau_p)$ is their time-dependent density, m_{eff} is their effective mass, τ_s is their momentum relaxation time, and e_0 denotes the elementary charge. The term $\mu_0 = e_0\tau_s/m_{\text{eff}}$ can be identified with their dc mobility. We measured the transient conductivity spectra for several pump-probe delays and found that their shape does not change significantly while their amplitude decreases with increasing pump-probe delay. This means that the momentum relaxation time τ_s is time independent and the observed decay of the pump-probe scans [Fig. 2(b)] reflects the population decay of free charge carriers only. The population decay can be well described by a single-exponential with a decay time τ_{decay},

$$n(\tau_p) = n_0 \exp(-\tau_p/\tau_{\text{decay}}) + n_b, \tag{3}$$

where n_0 is the initial population of charge carriers and the plateau value n_b represents their population at long pump-

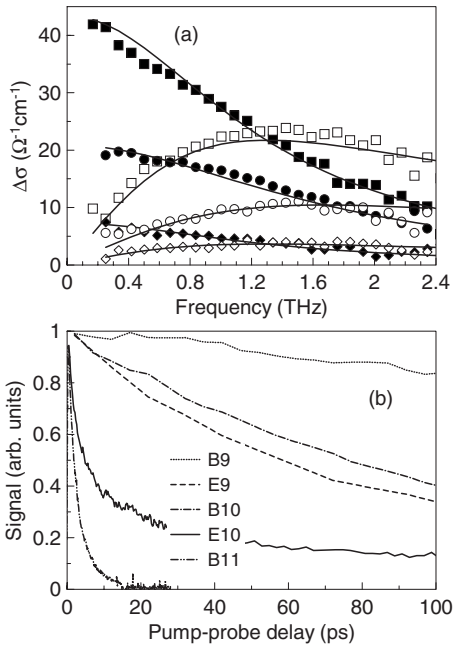

FIG. 2. (a) Examples of transient conductivity spectra of the E9 (squares: τ_p=10 ps; diamonds: τ_p=400 ps) and E10 sample (circles: τ_p=3 ps). Solid symbols: real part; opened symbols: imaginary part. The lines represent fits by the Drude model [Eq. (2)]. (b) Normalized pump-probe scans measured in the samples exhibiting slow dynamics.

probe delays ($\tau_p \gg \tau_{\text{decay}}$), which arises mainly due to trap filling.

The parameters τ_s, τ_{decay}, and μ_0 obtained by fitting the transient conductivity spectra and pump-probe scans for all samples are summarized in Table I along with the corresponding excitation densities n_0. The initial concentration of carriers n_0 obtained from the fits of experimental spectra agree well—within 20%—with those estimated from the absorbed photon flux.

The dynamics of the E11 and B12 samples are very fast compared to the terahertz pulse duration (the decay of pump-probe scans occurs on a subpicosecond time scale), therefore it could not be analyzed within the quasistatic approximation and the two-dimensional frequency domain approach was applied for the data analysis. The amplitude of the transient conductivity is shown in Figs. 3(a) and 3(d). Its shape closely resembles the Drude response, which in the two-dimensional frequency space reads[20]

$$\Delta\sigma(f,f_p) = \frac{n_0 e_0^2}{m_{\text{eff}}} \frac{1}{\frac{1}{\tau_s} + \frac{1}{\tau_{\text{decay}}} - 2\pi i f} \frac{1}{\frac{1}{\tau_{\text{decay}}} - 2\pi i f_p}. \quad (4)$$

Similarly as in the case of the slow dynamics, the shape of the spectra as a function of the frequency f determines the momentum relaxation time τ_s. The dynamical evolution manifests itself mainly in their shape along the f_p direction: the faster the dynamics is (i.e., the shorter the time τ_{decay} is), the more extended the spectrum becomes.[20] Fitting the complex two-dimensional spectra [Figs. 3(b) and 3(e)] then yields the parameters τ_s and τ_{decay}; their values are displayed in Table I. The residuals defined as

$$\{[\text{Re}\,\Delta\sigma_{\text{fit}}(f,f_p) - \text{Re}\,\Delta\sigma_{\text{exp}}(f,f_p)]^2 + [\text{Im}\,\Delta\sigma_{\text{fit}}(f,f_p) - \text{Im}\,\Delta\sigma_{\text{exp}}(f,f_p)]^2\}^{1/2} \quad (5)$$

and displayed in Figs. 3(c) and 3(f) do not show any systematic deviation from white noise, which confirms the pertinence of the model and a good quality of the fit.

V. MODELING OF DYNAMICS IN THE E9 AND E10 SAMPLES

The dependence of the dynamics on the excitation intensity was investigated in the E9 and E10 samples in order to gain a deeper insight into the physical properties of these samples. We found that their spectral responses do not change significantly with increasing excitation intensity, which means that the momentum relaxation times and mobilities remain unaltered. By contrast, the dynamics slow down upon increasing the excitation intensity (Fig. 4), indicating that the trap filling occurs. The observed dynamics become more complex also owing to the diffusion of free carriers. Indeed, we can estimate the diffusion length as

$$l_{\text{diff}} \approx \sqrt{D\tau_{\text{decay}}} \approx \sqrt{\frac{k_B T \mu_0}{e_0} \tau_{\text{decay}}} \quad (6)$$

(D is the diffusion coefficient, k_B is the Boltzmann constant, and T is the temperature). From the data in Table I we find

TABLE I. Characteristics and properties of all investigated samples. The densities of defects resulting from host-atom displacements (n_{host}) and of implanted Br atoms (n_{Br}) were determined from the data in Fig. 1.

Sample	n_{host} (cm^{-3})	n_{Br} (cm^{-3})	n_0 (cm^{-3})	τ_s (fs)	μ_0 ($\text{cm}^2\ \text{V}^{-1}\ \text{s}^{-1}$)	τ_{decay} (ps)
B9	2×10^{16}	0	1.6×10^{17}	140	3000	490
E9	9×10^{16}	5×10^{12}	1.1×10^{17}	120	2600	70
B10	2×10^{17}	0	1.6×10^{17}	120	2700	100
E10	9×10^{17}	5×10^{13}	0.9×10^{17}	100	2100	5.5
B11	2×10^{18}	0	1.6×10^{17}	70	1600	2.6
E11	9×10^{18}	5×10^{14}	2.2×10^{17}	90	2100	1.2
B12	2×10^{19}	0	1.6×10^{17}	40	900	0.29

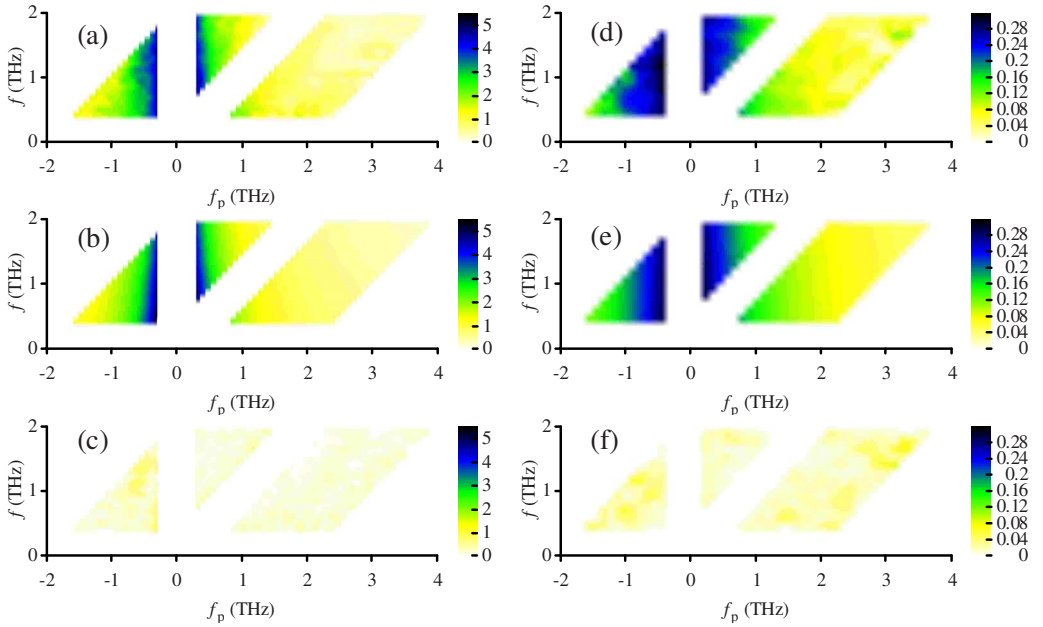

FIG. 3. (Color online) Amplitude of the transient conductivity spectra in [(a)–(c)] E11 and [(d)–(f)] B12 samples. Panels (a) and (d) show the transient conductivity determined from the experiment by the method described in Ref. 13. Panels (b) and (e) show the results of fits using the Drude model described by Eq. (4). Panels (c) and (f) show the residua which do not exhibit any additional characteristic features, thus indicating a good quality of the fit. The color scale indicates the conductivity in 10^3 Ω^{-1} m^{-1} ps.

that the diffusion lengths are ~690 and ~170 nm in the E9 and E10 samples, respectively. Since it is longer than or comparable with the absorption length of the excitation beam, a part of photogenerated carriers diffuses away from regions with significantly filled traps into those with nearly empty traps.

To account for both trap filling and diffusion, we set up and numerically solved a set of partial differential equations describing this problem (the details are provided in the Appendix). The model contains only four unknown parameters: lifetimes of electrons and holes (τ_e and τ_h, respectively), density of traps N_t, and position of traps below the conduction-band minimum ΔE. Using these parameters, a set of two to three pump-probe scans measured at different excitation intensities can be well matched (Fig. 4). The values of the fitting parameters are summarized in Table II. The capture cross sections for electrons and holes were calculated from the relation

$$\sigma_{e,h} = \frac{1}{N_t \tau_{e,h} v_{e,h}}, \tag{7}$$

where $v_{e,h} = \sqrt{3k_B T / m_{e,h}}$ is the thermal velocity of electrons and holes.

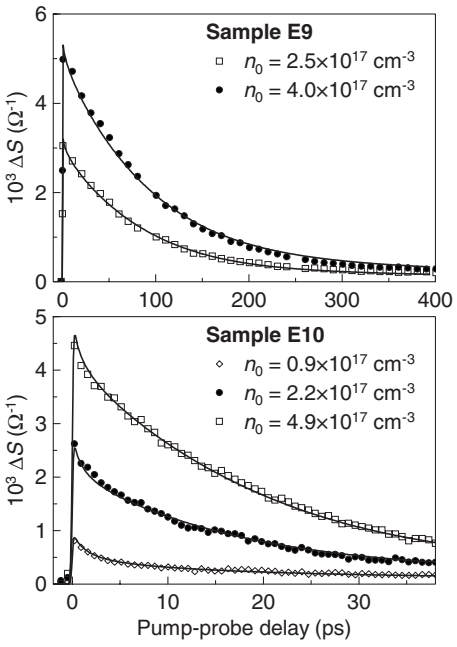

FIG. 4. Dynamics of the surface conductivity in the E9 and E10 samples as a function of excitation density. Points represent experimental data while lines are results of the numerical modeling.

VI. DISCUSSION

The trends in the carrier lifetime and mobility as a function of density of defects induced by ion irradiation are the same in the B and E samples (Fig. 5). We thus conclude that these properties are not significantly influenced by the implantation of the Br atoms, which are present only in the E samples. The only parameter determining the optoelectronic properties is thus the density of defects resulting from host-atom displacements.

The carrier lifetime is essentially inversely proportional to the density of defects induced by ion irradiation and its lowest value is 290 fs at the highest irradiation dose [Table I and Fig. 5(a)]. It should be noted that this simple law holds over four decades of the density of defects. Similar behavior was observed, e.g., in O^+-implanted silicon on sapphire[21] for doses $<10^{14}$ cm^{-2}, while for higher doses, the carrier life-

TABLE II. Properties of trapping sites in the E9 and E10 samples.

Sample	n_{host} (cm^{-3})	τ_e (ps)	τ_h (ps)	N_t (cm^{-3})	ΔE (eV)	σ_e (nm^2)	σ_h (nm^2)
E9	9×10^{16}	$<\tau_{decay}$	110	7.2×10^{15}	0.17	$\gtrsim$30	8
E10	9×10^{17}	2.3	26	3.4×10^{16}	0.11	30	8

time approaches a constant value of ~0.6 ps. From Fig. 5(a) it is evident that the doses we used are not high enough to reach the lifetime saturation regime in InP; we infer that irradiation by higher doses may produce a material with lifetimes significantly shorter than the observed 290 fs.

The electron mobility reaches 3000 $cm^2\ V^{-1}\ s^{-1}$ in the B9 sample, which contains the lowest density of defects created by ion irradiation. The same value was found in a nonirradiated InP wafer from the same batch. Such a level of mobility is an intrinsic property of the wafers used and it is only slightly lower than the Hall mobility of 5000 $cm^2\ V^{-1}\ s^{-1}$ reported for the best quality InP wafers.[22] The mobility then somewhat decreases with increasing density of defects [Table I and Fig. 5(b)]. A mobility as high as 900 $cm^2\ V^{-1}\ s^{-1}$ is still observed in the most heavily damaged B12 sample. The decrease in mobility originates from scattering of charge carriers on the defects induced by ion irradiation. This dependence can be understood in terms of Matthiessen's rule assuming that the rate of the carrier scattering on defects is inversely proportional to the carrier lifetime τ_{decay}. The effective carrier scattering time τ_s then reads

$$\frac{1}{\tau_s} = \frac{1}{\tau_{s,0}} + \frac{A}{\tau_{decay}}, \tag{8}$$

where $\tau_{s,0}$ is the carrier scattering time in a nonirradiated InP wafer and where the proportionality constant A can be identified with the ratio of cross sections for charge-carrier scattering and trapping; we find that $A \approx 7$. This very simple model qualitatively reproduces the mobility dependence; notably it shows that the decrease in mobility starts to occur for samples with carrier lifetimes comparable to the momentum relaxation times [Fig. 5(b)]. On the other hand, the rather large deviations may indicate that the scattering cross section of traps (or equivalently, the parameter A) depends on the trap occupation and on the density of radiation induced defects.

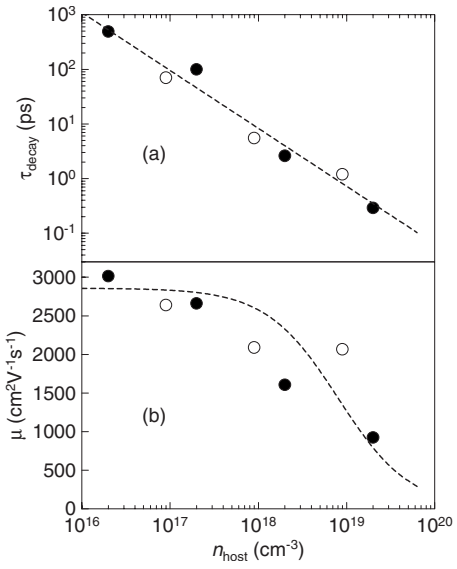

FIG. 5. Plot of (a) carrier decay time and (b) of mobility as a function of the density of defects resulting from host-atom displacements n_{host}. Filled circles represent B samples; opened circles stand for E samples. The dashed line in (a) indicates the trend of the data ($\tau_{decay} \propto 1/n_{host}$; the dashed line in (b) indicates the mobility calculated from Eq. (8).

A more detailed insight into the ultrafast dynamics was gained in the case of the E9 and E10 samples. In both cases, it was found that the density of traps is more than by an order of magnitude lower than that of host-atom displacements calculated by SRIM simulations. At the same time, the capture cross sections in both samples are comparable and relatively high. These results may be related to a particular nature of defects created by heavy-ion irradiation indicating that the defects are correlated and that they form clusters with a mean size of roughly ten point defects. The observed low density of traps may be also attributed to annealing processes that occur a few picoseconds after the ion irradiation and that are not taken into account by the SRIM simulation.

Due to the low density of defects in the E9 sample, trap filling occurred even for the lowest excitation densities used in our experiments. The electron lifetime thus could not be determined precisely for this sample. For the same reason, the lifetimes τ_{decay} in Table I for the B9 and B10 samples do not correspond to the electron lifetimes τ_e and the recombination of trapped electrons with free holes plays a significant role in this decay. For the samples with higher irradiation dose (B11, E11, and B12), $n_b \approx 0$ in Eq. (3) and we estimate that the trap density is higher than the initial carrier density; therefore τ_{decay} is a reasonable approximation of τ_e.

VII. CONCLUSIONS

By using time-resolved terahertz spectroscopy, we have characterized carrier lifetimes and mobilities in several Br^+-bombarded InP samples. Within irradiation doses from 10^9 to 10^{12} cm^{-2}, the carrier lifetime is inversely proportional to the density of the host-atom displacement defects. The mobility decreases with the irradiation dose due to additional scattering on the host-atom displacement defects. In the most irradiated sample, the carrier lifetime is reduced by three orders of magnitude whereas the mobility of carriers is only reduced by a factor of 3.3 compared to the as-grown sample. It was also found that implantation of Br atoms does not significantly influence the carrier lifetime and mobility.

A model of carrier dynamics including carrier trapping, trap filling, and carrier diffusion was developed to gain a

deeper insight into electron and hole dynamics. This allowed us to extract the density of traps along with electron and hole lifetimes in selected samples. Owing to the subpicosecond lifetimes combined with relatively high mobilities in the most heavily irradiated samples, the heavy-ion irradiated InP appears as a promising material for ultrafast optoelectronic applications.

ACKNOWLEDGMENTS

The financial support by the Ministry of Education of the Czech Republic (Project No. LC-512), by the Czech Science Foundation (Project No. 202/09/P099), by the Academy of Sciences Grant Agency (Project No. A100100902), and by the EGIDE-CNRS is gratefully acknowledged.

APPENDIX

The depth profiles of transient densities of free electrons, trapped electrons, and free holes (n_e, n_t, and n_h, respectively) and their time evolution are described by a set of coupled diffusion equations,

$$\frac{\partial n_e}{\partial t} = D_e \frac{\partial^2 n_e}{\partial z^2} - \frac{n_e}{\tau_e}\left(1 - \frac{n_t}{N_t}\right) + g_e n_t,$$

$$\frac{\partial n_t}{\partial t} = \frac{n_e}{\tau_e}\left(1 - \frac{n_t}{N_t}\right) - \frac{n_h}{\tau_h}\frac{n_t}{N_t} - n_t(g_e + g_h),$$

$$\frac{\partial n_h}{\partial t} = D_h \frac{\partial^2 n_h}{\partial z^2} - \frac{n_h}{\tau_h}\frac{n_t}{N_t} + g_h n_t, \tag{A1}$$

where τ_e and τ_h are lifetimes of electrons and holes, respectively, D_e and D_h are their diffusion coefficients, and N_t is the density of traps. These equations account for the diffusion of carriers, their trapping, and trap filling. Lateral diffusion is not considered since a broad and homogeneous initial distribution is generated in the experiment. The electron and hole release rates g_e and g_h are determined from a Shockley-Read model,[23]

$$g_e = \frac{1}{\tau_e}\frac{N_e}{N_t}\gamma_t \exp\left(-\frac{\Delta E}{k_B T}\right),$$

$$g_h = \frac{1}{\tau_h}\frac{N_h}{N_t}\gamma_t^{-1} \exp\left(-\frac{E_g - \Delta E}{k_B T}\right), \tag{A2}$$

which additionally depends on effective density of states of electrons and holes (N_e and N_h), band gap of the semiconductor E_g, and position of traps below the conduction-band minimum ΔE. The degeneracy factor γ_t is assumed to be unity. The traps are initially empty while the initial population of electrons and holes follows an exponential profile due to the absorption of the excitation beam,

$$n_{e,h}(z, t=0) = n_0 \exp(-\alpha z),$$

$$n_t(z, t=0) = 0. \tag{A3}$$

The boundary conditions require no flux through the sample surface ($z=0$).

A quantity directly comparable with the measured pump-probe scans is the surface conductivity, which reads

$$S(\omega, \tau_p) = e_0 \int_0^L [\mu_e(\omega) n_e(z, \tau_p) + \mu_h(\omega) n_h(z, \tau_p)] dz, \tag{A4}$$

where $L \gg l_{\mathrm{dif}}$. The surface conductivity is further convoluted with the temporal profile of the excitation beam to correctly describe the signal around $\tau_p = 0$.

Most of the parameters in the above equations are known from literature.[22] These equations are solved for a set of excitation fluences which differ by n_0 in Eq. (A3). Fitting a set of pump-probe scans measured at different excitation fluences then yields the four unknown parameters: τ_e, τ_h, N_t, and ΔE.

[1] A. Krotkus and J.-L. Coutaz, Semicond. Sci. Technol. **20**, S142 (2005).
[2] S. Gupta, J. F. Whitaker, and G. A. Mourou, IEEE J. Quantum Electron. **28**, 2464 (1992).
[3] B. W. Liang, P. Z. Lee, D. W. Shih, and C. W. Tu, Appl. Phys. Lett. **60**, 2104 (1992).
[4] A. Gasparotto, A. Carnera, C. Frigeri, F. Priolo, B. Fraboni, A. Camporese, and G. Rossetto, J. Appl. Phys. **85**, 753 (1999).
[5] C. Carmody, H. H. Tan, C. Jagadish, A. Gaarder, and S. Marcinkevičius, J. Appl. Phys. **94**, 1074 (2003).
[6] T.-A. Liu, M. Tani, M. Nakajima, M. Hangyo, K. Sakai, S. Nakashima, and C.-L. Pan, Opt. Express **12**, 2954 (2004).
[7] P. Mounaix, M. Tondusson, N. Chimot, J. Mangeney, K. Blary, and J. F. Lampin, Electron. Lett. **42**, 879 (2006).
[8] L. Joulaud, J. Mangeney, N. Chimot, P. Crozat, G. Fishman, and J. C. Bourgoin, J. Appl. Phys. **97**, 063515 (2005).
[9] C. Messner, H. Kostner, R. A. Höpfel, and K. Unterrainer, J. Opt. Soc. Am. B **18**, 1369 (2001).
[10] Ch. A. Schmuttenmaer, Chem. Rev. (Washington, D.C.) **104**, 1759 (2004).
[11] F. A. Hegmann, O. Ostroverkhova, and D. G. Cooke, in *Photophysics of Molecular Materials*, edited by Guglielmo Lanzani (Wiley, New York, 2006) pp. 367–428.
[12] M. C. Beard, G. M. Turner, and C. A. Schmuttenmaer, J. Appl. Phys. **90**, 5915 (2001).
[13] H. Němec, F. Kadlec, C. Kadlec, P. Kužel, and P. Jungwirth, J. Chem. Phys. **122**, 104504 (2005).
[14] J. P. Biersack and L. G. Haggmark, Nucl. Instrum. Methods **174**, 257 (1980).
[15] P. Kužel, F. Kadlec, and H. Němec, J. Chem. Phys. **127**, 024506 (2007).
[16] H. K. Nienhuys and V. Sundstrom, Phys. Rev. B **71**, 235110

(2005).
[17] J. T. Kindt and Ch. A. Schmuttenmaer, J. Chem. Phys. **110**, 8589 (1999).
[18] H. Němec, F. Kadlec, and P. Kužel, J. Chem. Phys. **117**, 8454 (2002).
[19] M. Van Exter and D. Grischkowsky, Appl. Phys. Lett. **56**, 1694 (1990).
[20] H. Němec, F. Kadlec, S. Surendran, P. Kužel, and P. Jungwirth, J. Chem. Phys. **122**, 104503 (2005).
[21] F. E. Doany, D. Grischkowsky, and C.-C. Chi, Appl. Phys. Lett. **50**, 460 (1987).
[22] M. Levinshtein, S. Rumayantsev, and M. Shur, *Handbook Series on Semiconductor Parameters 2* (World Scientific, Singapore, 1999).
[23] W. Shockley and W. T. Read, Phys. Rev. **87**, 835 (1952).